Case Studies in Construction Materials 19 (2023) e02535

Contents lists available at ScienceDirect

Case Studies in Construction Materials

journal homepage: www.elsevier.com/locate/cscm

Establishing pyrolysis kinetics for fire modelling and thermal analysis of polymeric cladding materials used in high-rise buildings

Md Delwar Hossain [a,b,*], Swapan Saha [a], Md Kamrul Hassan [a], Anthony Chun Yin Yuen [c], Cheng Wang [d]

[a] School of Engineering, Design and Built environment, Western Sydney University, Penrith, NSW 2751, Australia
[b] Department of Textile Engineering, Dhaka University of Engineering & Technology, Bangladesh
[c] Department of Building Environment and Energy Engineering, The Hong Kong Polytechnic University, Hong Kong
[d] School of Mechanical and Manufacturing Engineering, University of New South Wales, Sydney 2052, Australia

ARTICLE INFO

Keywords:
Aluminium Composite Panels
Cladding
Pyrolysis kinetics
Cone calorimeter
Fire modelling
High-rise building

ABSTRACT

This research paper presents a comprehensive analysis of kinetics data concerning with the core materials of Aluminium Composite Panels (ACPs), with a specific focus on composite materials comprising mineral fillers and organic polymers. The study addresses the current scarcity of kinetics data for cladding panel core materials, particularly those with complex compositions involving mineral fillers and organic polymers, which poses a significant challenge for accurate fire modelling. The study aims to extract essential parameters, including activation energy, pre-exponential factors, and reaction orders, essential for precise fire modelling. This study involves Thermogravimetric Analysis (TGA) on three distinct cladding core materials, namely, ACP-1, ACP-2, and ACP-3, featuring varying proportions of organic polymer content (100%, 30%, and 7%) and exposure to different heating rates (5, 10, 15, and 20 K/min). By employing both model-free and model-based techniques in conjunction with TGA analysis, the study successfully derives kinetics data aligned with specific pyrolysis reaction stages. To validate the extracted kinetics data, the study conducted experimental tests utilising a Cone calorimeter. The results from these experiments showcased a strong correlation between fire performance parameters such as Total Heat Release (THR), Effective Heat of Combustion (EHC), and Mass Loss Rate (MLR) and the proportion of polymer in the cladding composites. Furthermore, the study examined the implications of the derived kinetics data within the Fire Dynamics Simulator (FDS). The insights gained from this research substantially contribute to our comprehension of core material kinetics in ACPs, while also offering valuable input for fire dynamics simulations, thereby enhancing fire safety modelling and practices knowledge in the field of construction materials and design.

1. Introduction

Building cladding systems are designed for aesthetics and energy efficiency. It is also a vital component of green construction and

* Corresponding author at: School of Engineering, Design and Built environment, Western Sydney University, Penrith, NSW 2751, Australia.
E-mail addresses: md.hossain@westernsydney.edu.au (M.D. Hossain), s.saha@westernsydney.edu.au (S. Saha), k.hassan@westernsydney.edu.au (M.K. Hassan), anthony-cy.yuen@polyu.edu.hk (A.C.Y. Yuen), c.wang@unsw.edu.au (C. Wang).

https://doi.org/10.1016/j.cscm.2023.e02535
Received 22 July 2023; Received in revised form 20 September 2023; Accepted 2 October 2023
Available online 4 October 2023

carbon neutrality. However, combustible and flammable core materials in Aluminium Composite Panels (ACPs) can pave the way for rapid fire spread [1]. Recent high-rise building fires indicate the warnings of the vulnerability of these ACP cladding panels [1,2]. There were various ACP cladding panels on the market, most of them with low-density polyethylene (LDPE) and low-density polyethylene vinyl acetate (LDPE-VA) cores ranging from roughly 10–100% (in wt%), with and without fire retardant mineral fillers [3]. Fire retardant mineral fillers such as aluminium hydroxide ($Al(OH)_3$) and magnesium hydroxide ($Mg(OH)_2$) are commonly used in the core composites of ACP cladding panels [3–5]. Following the Grenfell fire incident, a series of full-scale tests were conducted to classify ACPs based on their core materials and calorific value [1]. Category 1 represents materials with limited combustibility, with a calorific value of less than 3 MJ/kg and less than 7% Polyethylene (PE). In contrast, Category 2 and Category 3 denote materials with limited flame retardancy and non-flame retardancy, respectively, with Category 2 containing approximately 30% PE and Category 3 comprising nearly 100% PE. The calorific values for Category 2 range from 3 to 35 MJ/kg, while Category 3 exhibits calorific values exceeding 35 MJ/kg [1]. The full-scale fire testing approach has been widely employed in many countries to assess the fire performance of cladding systems, encompassing cladding panels, insulation, and fastening components [6,7]. Conducting a full-scale test that accurately simulates a cladding fire necessitates well-equipped fire laboratories with extensive infrastructures [8,9]. Moreover, these tests typically incur high costs, require extensive planning, result in substantial environmental pollutant emissions, and vary risk assessment criteria across different countries [10–13]. Furthermore, conducting a full-scale test to analyse the flammability of existing building claddings is impractical due to the substantial quantities of test materials required, resulting in significant expenses [4]. In Australia, more than 3400 buildings were reported as risky buildings, and analyses were needed for the fire performance of these building cladding systems [14]. Understanding the fire hazards associated with 3400 building claddings through full-scale tests can be an expensive and time-consuming process. However, numerical fire modelling offers a potential alternative method to assess the fire hazards of these building claddings. This modelling approach provided a cost-effective alternative to conducting expensive experimental tests for analysing the fire behaviour of materials. To accurately predict the fire behaviour of a material numerically, it is necessary first to develop a pyrolysis model. The accuracy of the pyrolysis modelling, on the other hand, is largely dependent on the kinetics input data or kinetics triplets, which are the activation energy (E_a), pre-exponential factor (A), and reaction model ($f(\alpha)$). The most vulnerable core materials in ACPs are LDPE and its composites. There are several research studies on the kinetics triplet analysis of low-density polyethylene (LDPE) [15–18]. Dubdub et al. [17] utilised artificial neural network (ANN) to predict the kinetics triplets using model-free methods. The predicted activation energy ranged between 193 and 195 kJ/mol [17]. Aboulkas et al. [16] studied the pyrolysis kinetics of LDPE for polymer recycling schemes on an industrial scale. The study proposed a "contracting sphere" model with activation energy ranging from 179 to 188 kJ/mol [16]. Recently, Budrugeac et al. [18] studied the multivariate nonlinear regression methods for analysing the kinetics scheme. Das et al. [15] used different iso-conversional methods to analyse the thermal degradation kinetics of LDPE. Previous research on kinetics data has predominantly focused on 100% LDPE (Low-Density Polyethylene), leaving limited information available for LDPE core composites containing 10% and 30% mineral fillers. The lack of kinetics data for these core materials is a crucial gap that needs to be addressed to effectively investigate the fire performance of fire-retardant cladding panels through numerical modelling.

Chen et al. [19] utilised kinetics data for fire modelling a two-storey building with ACP cladding (100% LDPE). Drean et al. [20,21] developed full-scale ACP cladding system fire models and suggested that more accurate input data is needed for more accurate modelling. However, the study did not consider the kinetic properties as input data during fire modelling. Comprehensive pyrolysis models have proven flexible in describing the combustible nature of solids, and the lack of accurate kinetics parameters hindered the model prediction accuracy even with comprehensive fire modelling [22]. To the author's knowledge, there is currently a lack of available kinetic parameters for the different core materials of ACPs. To address the above research gap, this study aims to establish quality kinetics data and benchmark their accuracies compared to experiment data from TGA. Kinetics NEO, a cutting-edge kinetic software, was used to calculate critical kinetic parameters as a derived kinetic triplet. To assure accuracy, the study employs both model-free and model-based kinetic approaches [23]. This study also utilises the kinetics in the FDS model coupled with the pyrolysis model to study the fire development and compare it against Cone calorimeter data. In addition, simulations were carried out to estimate the mass loss of various cladding materials when subjected to different fire curves.

2. Materials and methods

2.1. Materials

Test materials were collected from three different commercial cladding products, and details were listed in Table 1. ACP-1 with 100% LDPE is used and reported extensively in Australia and other parts of the world as a cladding panel in high-rise buildings [4,24].

Table 1
Materials details of test samples.

Sample code	Polymer*	Polymer† (wt%)	Mineral filler*	Mineral filler† (%)	b* (mm)	ρ* (kg/ m^3)	k* (W/m·K)	C_P* (J/g·K)
ACP-1	LDPE	100%	-	0%	3	917	0.28	2.164
ACP-2	LDPE-VA	30%	ATH	70	3	1617	0.33	1.531
ACP-3	LDPE	7%	ATH+ Calcite	93	3	1650	1.00	1.055

Thickness = b, Density = ρ, Thermal conductivity= k, Specific heat= C_P, Data from manufacturer = †,wt = weight and Measured data = *.

ACP-2 and ACP-3 were the only ACP cladding panels currently allowed on new or newly refurbished residential buildings in Australia [25].

ACPs typically consist of a core material with a thickness of 3 mm sandwiched between two aluminium layers, each with a thickness of 0.5 mm. These layers were bonded together using a thin layer of adhesive [26]. The core materials of ACP-2 and ACP-3 were usually a mixture of polymer (LDPE and LDPE-VA) with different levels of fire-retardant mineral fillers (ATH and Calcite) to achieve fire-retardant properties to slow down and reduce the intensity of fire spread in the buildings. ACP-2 and ACP-3 comprise approximately 30% and 7% of the polymer by the weight of total core composites. The density and thermal conductivity data were obtained from the materials suppliers. The density of 917 kg/m^3 and a thermal conductivity of 0.28 W/m·K was found for ACP-1, while for ACP-2, the density of 1617 kg/m^3 and a thermal conductivity of 0.33 W/m·K was found. ACP-3 contained a density of 1650 kg/m^3 and a thermal conductivity of 1.00 W/m·K. To determine the specific heat, the study utilized Differential Scanning Calorimetry (DSC), and calculated the specific heat capacity (C_p) as a function of temperature for each sample [27]. The C_p values were found to be 2.164 J/g·K for ACP-1, 1.531 J/g·K for ACP-2, and 1.055 J/g·K for ACP-3. However, chemical formulas and compositions of core materials are frequently trade secrets, and they differ from manufacturer to manufacturer and need to be confirm by morphological analysis [28]. In Fig. 1, the core samples of all the ACPs were illustrated, with an inset providing a top view of each sample.

2.2. Thermal degradation analysis

This study utilised Simultaneous Thermal Analysis (STA) to examine the variations in thermal degradation patterns among the different test samples. STA analysis was performed using Netzsch STA449C Jupiter instrument analyse to analyse the thermal decomposition steps to obtain kinetics parameters that fit the experimental data. Experimental heating rates of 5, 10, 15, and 20 °C/min were selected based on recent research studies to analyse the various thermal decomposition stages [29–31]. The characterisation process was carried out under nitrogen atmosphere. The flow rate was 50 mL/min. The overall analysing temperature ranging from 35 °C to 1000 °C was used. Depending on the sample type and temperature range needed, samples were loaded into either aluminium or platinum crucibles, with sample weights ranging from 10 ± 0.2 mg [32,33]. Samples were taken from a cross-section area of three different places to ensure the representation of each component in the mixture. To ensure reproducibility, duplicate runs were periodically conducted for each heating rate and material.

2.3. Pyrolysis kinetics and data extraction

Pyrolysis refers to the thermal degradation of a material without the presence of oxygen, resulting in the generation of volatile combustibles and non-combustibles. The volatile combustibles can trigger ignition, sustain combustion, and facilitate the spread of flames across the material. To appropriately estimate the fire behaviour of an ACP cladding system, it is critical to collect pyrolysis kinetics data for each material utilised in cladding systems, which has not been substantially investigated thus far. Researchers are increasingly using STA technique to investigate the pyrolysis kinetics of various building materials. [30,34,35]. Both model-free and model-based techniques can be used for analysing the kinetics parameters for different reasons, i.e., reaction steps analysis, process optimisation, temperature prediction for different steps, and heating rates [15,36]. Model-based and model-free methods can then be implemented to characterise pyrolysis kinetics data based on Arrhenius's law of reaction. Sánchez-Jiménez et al. [37] discovered that

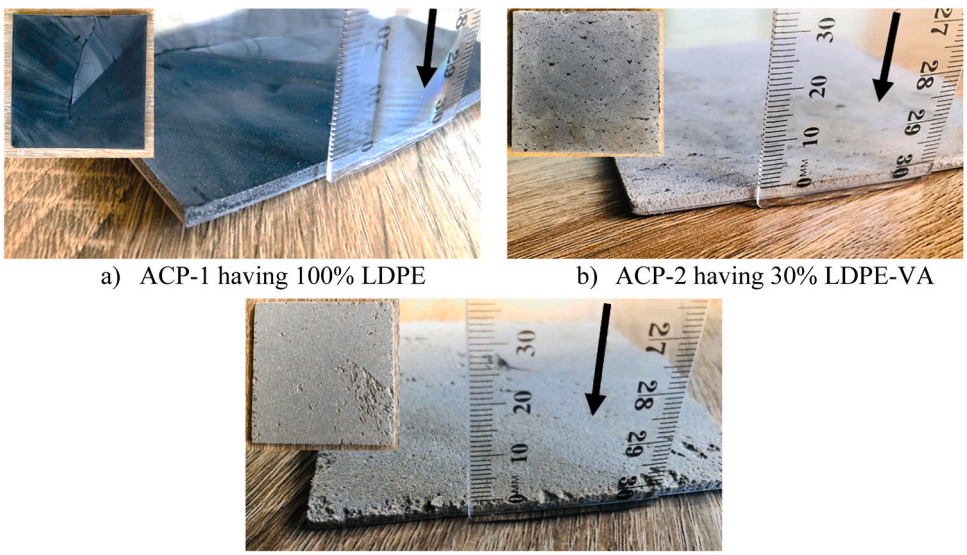

Fig. 1. Different materials of the cladding system.

using a model-based method to compute significantly different kinetic parameter values could more accurately match experimental data. However, the uncertainty in retrieving kinetic parameters can be reduced using model-free methods.

The reaction rate in model-free method can be analysed using a single kinetic equation (Eq. 1) concerning reaction conversion (α).

$$\frac{d\alpha}{dt} = A \quad (\alpha) \quad \exp\left[-\frac{E_a(\alpha)}{RT}\right] f(\alpha) \tag{1}$$

Where, reaction rate $= \frac{d\alpha}{dt}$ (1/s), time $= t$ (s), absolute temperature $= T$ (K), the gas constant $= R$ (8.314 J /K·mol), and the function of kinetic reaction is $f(\alpha)$. Table 2 lists the model-free techniques taken into account in this work for kinetics analysis. Moreover, individual kinetic equations can represent each reaction step employed in the model-based kinetic analysis. Where reactant concentration is e_j, specific step denoted by j and the product concentration is p_j.The reaction rate of j steps can be described as follows:

$$(\text{Reaction } rate)_j = A_j \bullet f_j(e_j, p_j) \exp\left(-\frac{E_{aj}}{RT}\right) \tag{2}$$

Table 3 summarizes the frequently utilized reaction types in Kinetics NEO, where each step is described by its corresponding function, $f_j\left(e_j, p_j\right)$.

A systematic framework was used in Fig. 2 for extracting kinetics data from STA analysis. The framework was adapted from our previous research work, and details can be found in [38]. At first, preliminary pyrolysis reaction steps were identified for determining the suitable model types through the analysis of TGA and DTG curves of each sample. Curve fitting was then performed to define an appropriate model, allowing the identification of the optimal number of reaction steps for the tested samples. By carefully selecting experimental data and employing either model-free / model-based method, the kinetics triplets were utilised to measure various outputs, such as signals, conversion, and rate of conversion. The appropriate model selection for each type of sample was determined through statistical analysis and curve fitting. The Kinetics NEO software toolset was employed for all statistical analysis and curve fittings. For optimisation and curve fitting, the nonlinear least squares method was used during statistical analysis [23,39]. Statistical analysis involves calculating the coefficient of determination (R^2) and residual sum of squares (S^2) and performing an F-test with a right tail p-value of 0.05. The kinetics parameters were optimised using the least squares method for achieving the optimum coefficient of determination (R^2) between the experimental and simulated data. Further details regarding the well-known coefficient of determination (R^2) can be found elsewhere [40]. Different model-free and model-based methods were assessed by employing the F-test for analysing the suitability of modelling. It utilised the least square method using the non-symmetrical distribution for sampling for analysing the suitability of different methods. A higher F-test value indicates the model's unsuitability. Then, the best models were selected based on the overall statistical significance. Finally, the kinetics data were used for fire performance analyses using fire modelling.

2.4. Cone calorimeter tests

The reaction-to-fire tests were conducted accordance with ISO 5660 standards. These tests focused exclusively on the core materials, excluding the aluminium outer skin, as they represent the primary fire hazard [1]. Prior to testing, all samples were meticulously prepared, cut to dimensions of 100 mm × 100 mm × 3 mm, and wrapped in aluminium foil, leaving the upper surface exposed. The measurements were taken with the sample holder positioned horizontally under standard atmospheric conditions, maintaining a consistent nominal exhaust fan airflow rate of 0.0026 m^3 /s across all experiments. To ensure measurement precision and repeatability, triplicate samples of each material were subjected to an incident heat flux of 50 kW/m^2. The study will analyse the reaction-to-fire properties, such as time to ignition (TTI), peak heat release rate (pHRR), time to peak heat release rate (t_{pHRR}), and total heat release (THR), which are considered critical parameters for fire assessment and regulatory screening of the ACP claddings used in buildings.

Table 2
List of model-free methods considered [37–39].

Methods	Types	Expression
Friedman (FR)	Differential	$\ln(\beta\frac{d\alpha}{dt}) = \ln[Af(\alpha)] - \frac{E}{RT}$
Ozawa-Flynn-Wall (OFW)	Integral	$\ln(\beta) = \ln\left(-\frac{AE}{R\ln(1-\alpha)}\right) - 5.331 - 1.052\frac{E}{RT}$
Kissinger-Akahira-Sunose (KAS)	Integral	$\ln(\frac{\beta}{T^2}) = \ln\left(-\frac{AR}{E\ln(1-\alpha)}\right) - \frac{E}{RT}$
Vyazovkin (VA)	Integral	$\Phi(E_a) = \sum_{i=1}^{n}\sum_{j\neq1}^{n}\frac{J(E_a, T_i(t_\alpha)}{J(E_a, T_j(t_\alpha)}$
		Where, $J(E_a, T_i(t_\alpha) = \int_{t_\alpha-\Delta\alpha}^{t_\alpha} \exp\left[\frac{-E_a}{RT_i(t)}\right]dt$

Table 3
List of model-based reaction types and related reaction equations considered [23].

Code	Function	Type of reaction
Fn	$f = (1-\alpha)^n$	n^{th} order reaction
Cn	$f = (1-\alpha)^n \bullet (1 + \mathrm{Kcat} \bullet \alpha)$	n^{th} order reaction with autocatalysis by product
Cnm	$f = (1-\alpha)^n \bullet (1 + \mathrm{Kcat} \bullet \alpha^m)$	n^{th} order reaction with m-Power autocatalysis by product
A2	$f = 2(1-\alpha) \bullet [-\ln(1-\alpha)]^{1/2}$	2-D nucleation according to Avrami
A3	$f = 3(1-\alpha) \bullet [-\ln(1-\alpha)]^{2/3}$	3-D nucleation according to Avrami
An	$f = n(1-\alpha) \bullet [-\ln(1-\alpha)]^{n-1/n}$	n-dimensional(D) nucleation according to Avrami− Erofeev
KS	$\text{Reaction rate} = A \bullet (1-\alpha)^n \left[\exp(-\frac{E}{RT}) + Kcat \bullet \alpha^m \bullet \exp(-\frac{E2}{RT})\right]$	Kamal-Sourur equation

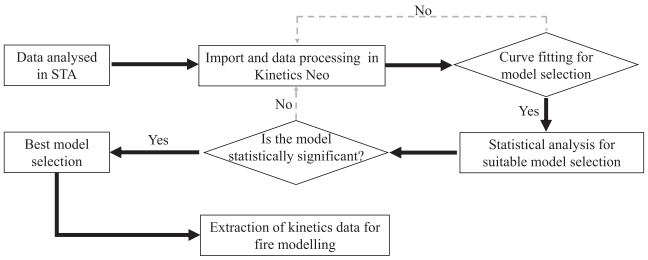

Fig. 2. Framework for kinetics data extractions of cladding materials [38].

2.5. Cone calorimeter modelling using FDS

Pyrolysis and combustion reactions were modelled in the small-scale Cone calorimeter for core materials of ACPs. The numerical simulation tool used in this study is the Fire Dynamics Simulator (FDS 6.7.9) [41]. FDS is a CFD modelling tool developed by the National Institute of Standards and Technology (NIST) with LES and DNS solvers. For pyrolysis modelling the current study will use the Arrhenius law of reaction to specify the kinetics parameter and the general equation used in FDS [41].

2.5.1. Model setup

To avoid the complexity of simulating the cone heater and its corresponding shape to ensure that the desired heat flux is directed towards the target sample, an alternative approach is used directly applying an external heat flux to the sample surface, representing the cone heater. However, "EXTERNAL HEAT FLUX" function can be used in "SURF" properties to describe the virtual heat flux of the cone heater. The current study used the value of "EXTERNAL HEAT FLUX" = 50, which is assumed to be the equivalent value of the experimental incident heat flux of 50 kW/m^2. For the fuel and combustion efficiency, CO yield of 0.024 g/g and soot yield was 0.056 g/g was taken from the literature [21]. This study will use comprehensive pyrolysis model using FDS,allow modelling one or multiple chemical decomposition reactions [42]. The reaction rate of each chemical decomposition is calculated using the Arrhenius

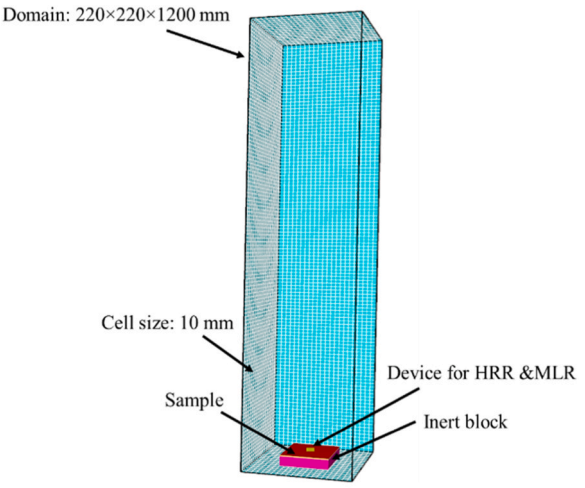

Fig. 3. Setup of Cone calorimeter in FDS simulation.

law. The input parameters utilised for the modelling were derived from the physio-thermal properties (Table 1) and the optimised kinetics data from the present study (Table 7). To simulate the fire plume region and capture the heating effect a domain of 220 mm (L) × 220 mm (W) × 1200 (h) mm was employed (Fig. 3). In the domain, the sample was created with a dimension of 100 mm × 100 mm and set up by the top surface of a solid block. Except for the top surface, the other surfaces of the sample were considered as insert surfaces during simulation to replicate the experimental condition of the Cone calorimeter. To ensure independence from the mesh, a mesh assessment is conducted, utilising a 10 mm cubic cell for gas phase computations. This choice yields comparable results to those obtained using a 5 mm cell size while maintaining a reasonable computational time. The cell size is determined through grid sensitivity analyses for the solid phase, and details can be found in (Table 4).

2.5.2. Mesh sensitivity

In this study, mesh sensitivity was analysed based on cell size. The cell size of the immediate fire region can be calculated based on the characteristic fire diameter (D^*) using the below equation [43].

$$D^* = \left(\frac{Q}{\rho_\infty T_\infty c_p \sqrt{g}}\right)^{2/5}$$

Where D^* is the characteristic fire diameter (m), Q is the heat release rate of the fire (kW), ρ_∞ is the ambient air density (1.2 kg/m^3), C_p is the specific heat capacity of air (1.0 kJ/kg K), T_∞ is the ambient air temperature (293 K), g is the gravitational acceleration (9.81 m/s^2).

The minimum requirement of mesh to fully capture the combustion behaviour was studied based on D* /δx value ranging between 4 and 16 to indicate the coarser to finer mesh. The 20 mm mesh size is used for D* /δx = 4. The 10 mm mesh size is used for D* /δx = 10 and 5 mm mesh size is used for D* /δx = 16. The details of cell size and number of cells can be found in Table 4. While the heat release rate (HRR) is the most critical parameter governing the fire intensity of the solid fuel, it has been implemented as the targeted variable for the mesh sensitivity test from the Fig. 4 it can be seen that there is a changes between the mesh of 20 mm and 5 mm. However, the 10 mm and 5 mm cell size showed significantly less difference. Therefore, for the purpose to maximise the efficiency while retaining reasonable simulation time cell size 10 mm is considered in this study.

2.6. Microscopy and elemental analysis

Scanning electron microscopy (SEM) was used to analyse the ACP core samples morphological structure at different states, i.e., solid and char. The analysis also helped to identify the presence of different mineral fillers in the core composites. Samples were imaged at 50x magnification with a backscatter detector on a Jeol 6510LV SEM. The accelerating voltage is used with a value of 25 kV. An Amptek energy dispersive spectroscopy (EDS) and Moran Scientific analysis software were also used for elemental microanalysis to determine the elements in the samples and any fillers. SEM and EDS results of ACP samples (ACP-1, ACP-2 and ACP-3) and their chars were reported in Fig. 5**,** respectively. After heating samples, ACP-1 showed a negligible amount of residual mass. Hence, no char analysis could be performed on these two samples. Sample ACP-1 (Fig. 5a) exhibited a homogeneous structure with no filler or additives. The EDS revealed that the material was mostly carbon (C) based (Fig. 5b). According to the materials section (Table 1), ACP-2 is made up of 30% LDPE-VA, with the rest being mineral filler. The morphological structure seen in the SEM image also confirms the presence of a composite material (Fig. 5c). Aluminium (Al) and oxygen (O) have noticeable peaks in the EDS spectrum, along with a small amount of carbon (C). The filler used in this material is the commonly used aluminium tri-hydroxide (Al $(OH)_3$), which is known as ATH (Fig. 5d). The residual char of ACP-2 samples (Fig. 5e) showed the presence of only Al and O, which could be the result of the conversion of ATH after heating (Fig. 5f). The loss of the carbon peak after being exposed to heat is the result of the organic part of the composites, which is 30% LDPE-VA. After heating, this component is thermally decomposed without no residue left. In ACP-3, visual observation from the microanalysis revealed two types of filler in the composite configuration: one resembling an eggshell structure and the other resembling solid beads (Fig. 5g). Labelled mineral fillers 1 and 2 were also discovered in the residual char (Fig. 5i). Filler 1 is primarily made up of calcium (Ca), aluminium (Al), and oxygen (O) components, according to the elemental analysis. Aluminium (Al), Oxygen (O), and Silicon (Si) are prominent in filler 2. (Fig. 5j). ATH and calcium carbonate ($CaCO_3$) or calcite were used in ACP-3 as mineral fillers, according to test data reported in Table 1. The presence of all the materials, i.e., LDPE-VA, ATH and $CaCO_3$, has been confirmed by Fourier transform infrared (FTIR) analysis (Appendix C -supplementary material).

Table 4
Different cell sizes and number of mesh.

Cell size	Number of cell	D* /δx
20 mm (0.02 m)	8640	4
10 mm (0.01 m)	58080	10
5 mm (0.005 m)	486000	16

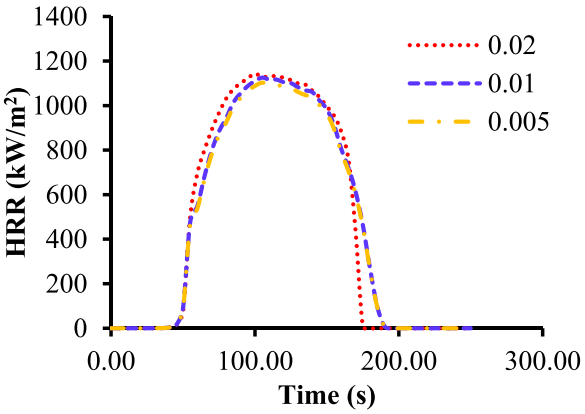

Fig. 4. Results of mesh sensitivity based on control variable HRR.

3. Results and discussion

3.1. Thermal degradation analysis

Thermal analysis was performed for identifying the onset temperature (T_o), peak temperature (T_p), end temperature (T_e) and mass residual (%) of ACP-1, ACP-2, and ACP (Table 5).

The onset temperature (T_o) was determined by locating the point where the curve's slope increased, a tangent line was drawn, and the intersection with the DTG curve was noted. The peak temperature (T_p) was identified as the highest point on the curve, representing the maximum rate of weight change. The end temperature (T_e) was determined by locating the point where the slope decreased, a tangent line was drawn, and its intersection with the DTG curve was observed. The procedure for analysing the T_o, T_p, and T_e from the experimental DTG curves was described in [15]. The T_o, T_p, and T_e values of DTG curve changes relates to heating rates and are discussed in [15,44]. The TGA and DTG results were utilised to estimate the samples' reaction steps. Though the visual inspection of the TGA curves is the simplest way to identify the multi-step reactions, but not consistently effective. A more effective way is kinetics analysis in primary model selection [45]. Specific reaction steps were discussed in a later section.

Fig. 6(a–c) shows the profiles of mass loss, mass loss rate and heat flow of test sample ACP-1. Single-step mass loss in the TGA curve and DTG curve confirm the single-step reaction of the ACP-1 [15,36]. As the heating rate increased, there was a shift to a higher peak temperature in the TG and DTG curves (Fig. 6a and b). Several researchers have attempted to explain and characterise these same phenomena [15,46]. It was noticed that ACP-1 decomposed entirely without leaving a solid residue (only 0.3%). However, two endothermic peaks were found in the DSC result **(**Fig. 6**c)**. The first peak is between 90 and 110 °C, and the second peak is between 450 and 500 ° C. As the first peak of DSC is endothermic and has no associated mass loss in the TG curve, it represents the melting point of the LDPE sample [47]. The second DSC peak was due to the thermal decomposition of the sample.

The TGA curve revealed three decomposition steps for ACP-2, with the DTG curve showing the same number of visible peaks. The detailed temperature scheme can be found in Table 5. Fig. 7(a–c) illustrates the relative mass loss, mass loss rate, and heat flow profiles of test sample ACP-2 at the different heating rates. ACP-2 was confirmed to be a composite of the polymer LDPE-VA and the mineral filler ATH (Supplementary Fig. S1**b**). The onset temperature (T_o) ranges from 222 to 238 ºC in the first decomposition step. The peak temperature was observed between 240 and 265 ºC. Only 3% mass loss has been noticed in this step and can be responsible for the partial transformation of ATH (also known as gibbsite) to ɣ-AlO (OH) (also known as boehmite), according to Eq. (3) [48]. For the second decomposition step, the peak temperature ranged between 318 and 340 ºC can be due to the decomposition of gibbsite to alumina polymorph χ-Al_2O_3 (see Eq. 4) [48] with a mass loss of 18%. The third decomposition has been noticed between the peak temperatures of 468–490 ºC and can be responsible for the thermal decomposition of LDPE-VA (low-density polyethylene vinyl acetate) with 30% mass loss [49]. The end temperature, T_e was between 481 and 555 ºC. The thermal decomposition of ATH in TGA has a three-step mass loss, with each step involving the loss of water, as shown in Eqs. (3–5) [48].

$$Al(OH)_3 \xrightarrow{190-220^{\circ}C} AlOOH + H_2O \tag{3}$$

$$2Al(OH)_3 \xrightarrow{220-380^{\circ}C} \chi - Al_2O_3 + 3H_2O \tag{4}$$

$$2AlOOH \xrightarrow{380-800^{\circ}C} \gamma - Al_2O_3 + H_2O \tag{5}$$

As the sample is a composite of LDPE-VA and a mineral filler material confirmed to be Al $(OH)_3$, a significant residual mass of 48% left is observed compared to the LDPE sample (ACP-1) with zero residual mass. From the DTG curve, the highest peak is found between 400 and 550 ºC. This step represents the thermal degradation of LDPE-VA of the composite matrix [49,50]. The peak endothermic heat flow is observed around 340 ºC in DSC curve, possibly due to the decomposition of gibbsite to alumina polymorph χ-Al_2O_3. ACP-3

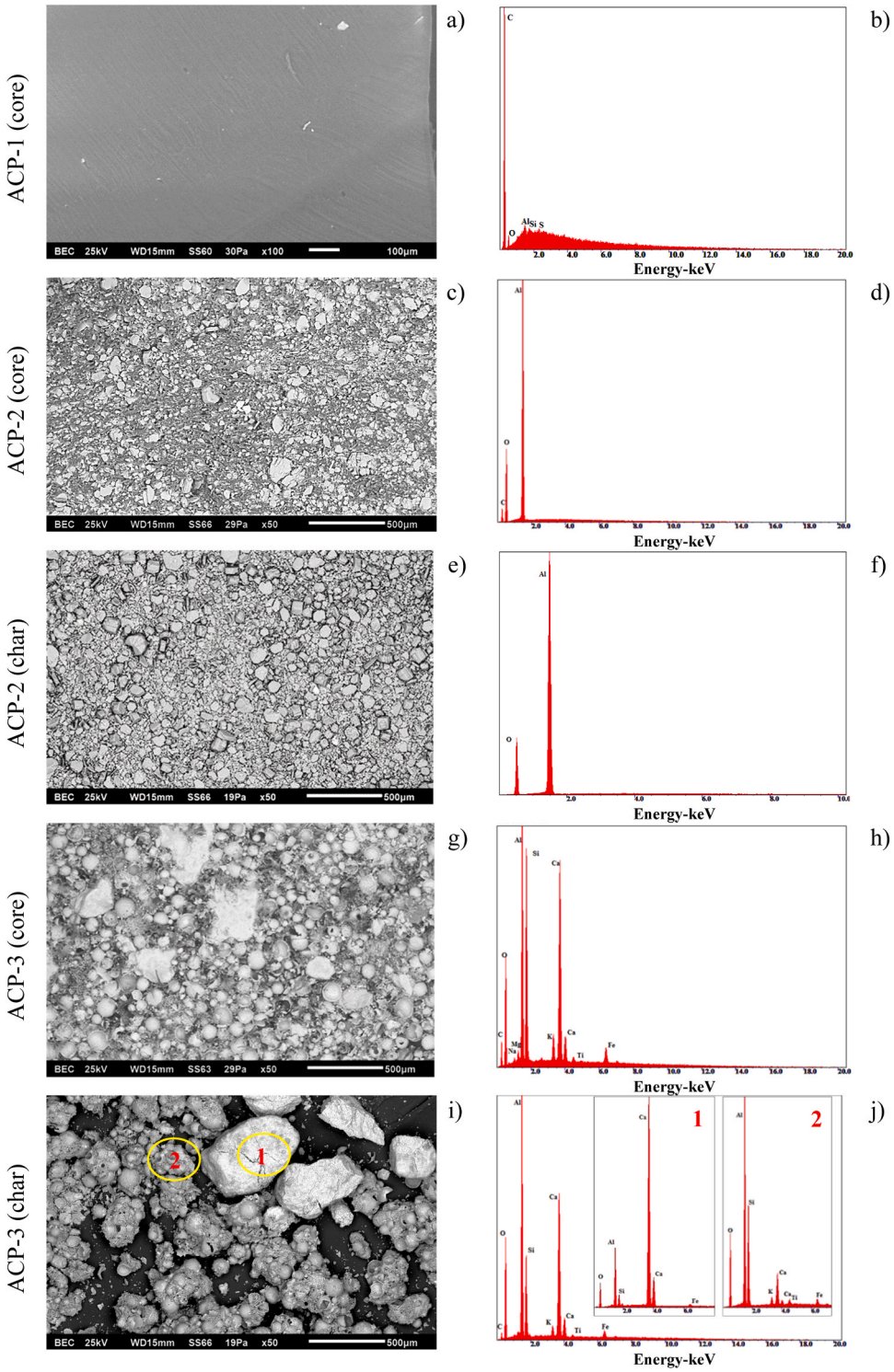

Fig. 5. Microscopy images (left) and elemental spectra (right) of cladding materials.

samples showed the same trend of three decomposition steps as ACP-2 (Fig. 8a-c). The samples of ACP-3 were composed of LDPE, ATH and $CaCO_3$ (Supplementary Fig. S1c). The average residual mass loss of 65% was observed in the TGA curve. The detailed temperature scheme in Table 5 shows that the onset temperature ranged from 240 to 253 °C. The peak temperature for the first decomposition step ranged between 290 and 315 °C due to gibbsite decomposition to χ-Al_2O_3. For the second decomposition step, the peak temperature

Table 5
Thermal analysis of cladding samples at different heat rates.

Material	Temperature range (°C)	Heating rate, (K/min)	Onset temperature, T_o (°C)	Peak temperature, T_P (°C)			End temperature, T_e (°C)	Mass residual %
				T_{P1}	T_{P2}	T_{P3}		
ACP-1	35–600	5	438	471	-	-	494	0.32
ACP-1	35–600	10	445	476	-	-	506	0.2
ACP-1	35–600	15	448	489	-	-	516	0.12
ACP-1	35–600	20	456	493	-	-	518	0.5
ACP-2	35–800	5	222	240	318	468	481	48
ACP-2	35–800	10	224	250	327	477	515	47.74
ACP-2	35–800	15	230	260	335	485	518	48.61
ACP-2	35–800	20	238	265	340	490	555	47.34
ACP-3	35–1000	5	240	290	455	780	838	64.41
ACP-3	35–1000	10	244	300	490	795	860	66.12
ACP-3	35–1000	15	246	310	490	815	886	65.85
ACP-3	35–1000	20	253	315	495	835	901	64.75

Here, T_o = onset temperature; T_p = peak temperature; T_e = end temperature, R= reaction steps

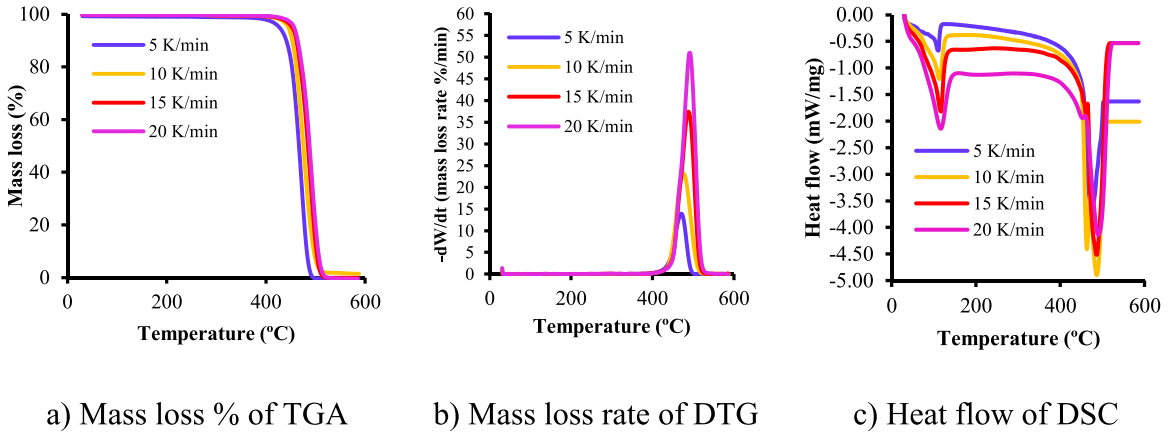

Fig. 6. Thermal degradation profiles for ACP-1 (100% LDPE).

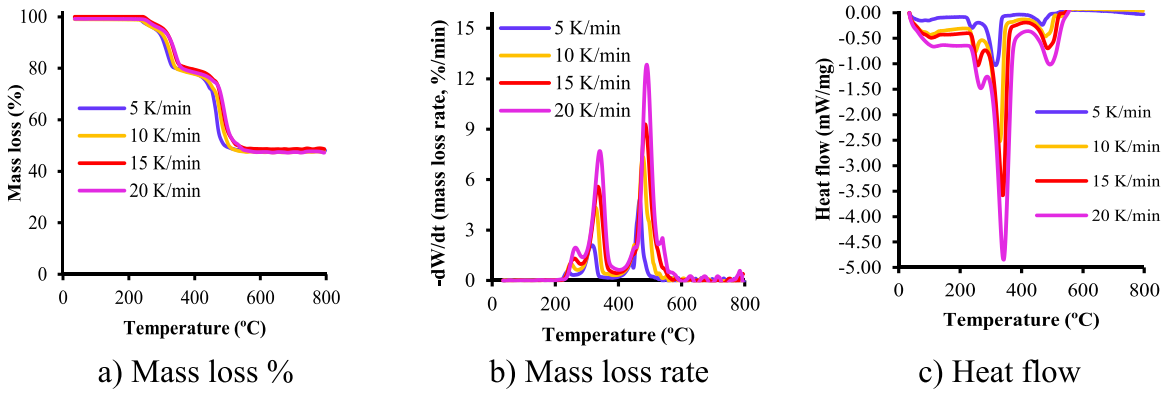

Fig. 7. Thermal degradation profiles of ACP-2 (30% LDPE).

ranging between 455 and 495 °C is possibly due to the decomposition of LDPE with a mass loss of around 7% and the third decomposition with a peak temperature of 780–835 °C can be responsible for the decomposition of $CaCO_3$ (see Eq. 6) [51]. The end temperature, T_e, ranged between 838 and 901 °C. The DTG curve (Fig. 8b) showed around 3.5 times less mass loss rate than ACP-2. In Fig. 8c, the highest endothermic peak at 835 °C of DSC could be associated with the decomposition of $CaCO_3$.

$$Ca(CO)_3 \overset{>600℃}{\rightarrow} CaO + CO_2 \quad (6)$$

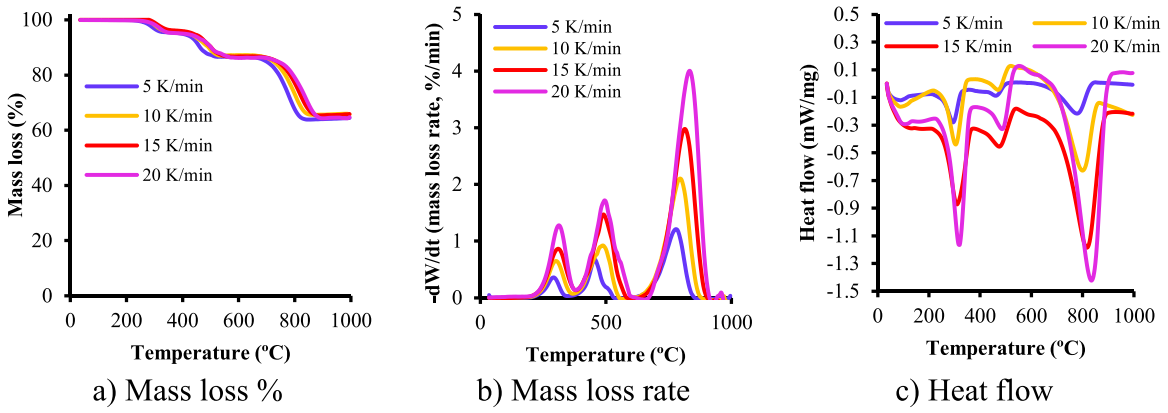

Fig. 8. Thermal degradation profiles of ACP-3 (7% LDPE).

3.2. Selection of kinetics model

The present study utilised the proposed framework described in Fig. 2 to select the model for each sample and analysis the kinetics parameters**.** All the kinetics analyses were based on the collected TGA mass loss results and the decomposition steps. Sample ACP-1, which consists of only LDPE, is modelled using iso-conversonal multipoint model-free methods (i.e., FR, OFW, KAS, VA and NOA) to analyse the kinetics parameters. The advantage of the model-free analysis is its simplicity and of avoiding errors connected with selecting a kinetics model [52]. However, ACP-2 and ACP-2 consist of multi-mixture elements in their core and have possibilities for individual reaction steps. In this type of condition, the model-free method is not suitable. Hence model-based methods were used (i.e. An, Cn, Cnm, Fn and KS) [53]. FR, NOA, and VA models overlapped in the curve fitting analysis (Fig. 9). In contrast, the shift and high amplitude in curve fitting were obtained with OFW and KAS. In FR, VA and NOA methods use the point values of the overall reaction rate or short time intervals [36]. However, OFW and KAS underestimate the E_a, when E_a increases with α. Because in both models, E_a assumes to be a constant value. As a result, conversion rate vs time curve variation can be observed [54]. Based on the results of model-based curve fitting, it is evident that the Cnm models exhibit excellent fit for ACP-2 (Fig. 10) and ACP-3 (Fig. 11), outperforming other models. To ensure results accuracy, it is crucial to conduct additional statistical analysis.

A comparative summary of the statistical analysis of the different kinetics models for the tested samples was provided in Table 6. The well-fitted model depends on a higher value of coefficient of determination, R^2, a lower *F*-test value, and a lower sum of deviation, S^2 [55,56]. Statistical analysis of ACP-1 revealed consistent trends among the FR, NOA, and VA models. *F*-test values ranged from 1 to 1.45, indicating the statistical significance of these models when compared to KAS (191) and OFW (10.68). The mean residual value was also smaller compared to KAS and OFW. The FR model has been chosen for the development of the model, considering its simplicity and the availability of relevant literature. For ACP-2 and 3, five different models were used: An, Cn, Cnm, Fn and KS. In the case of both samples, the Cnm model showed statistically more significance compared to the other models. The lower *F-test* value found for ACP-2 is 2.76 in the Cnm model. For ACP-3 the low *F*-test value was also observed for Cnm (19.13). The Cnm model, which utilises modified autocatalytic reactions, is particularly beneficial for analysing the kinetics data of polymer composites [57,58]. In this study, the kinetics of ACP-2 and ACP-3 were analysed using the Cnm model, which proved statistically significant based on curve fitting and analysis.

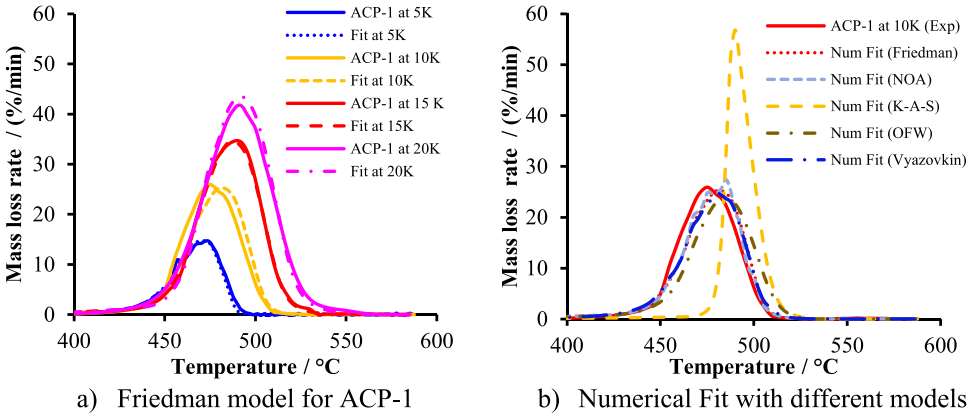

Fig. 9. DTG curve fitting of different models for ACP-1.

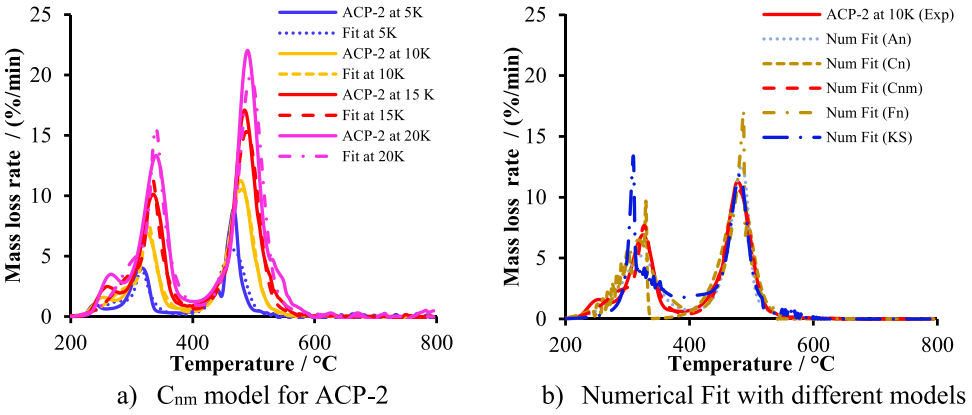

Fig. 10. DTG curve fitting of different models for ACP-2.

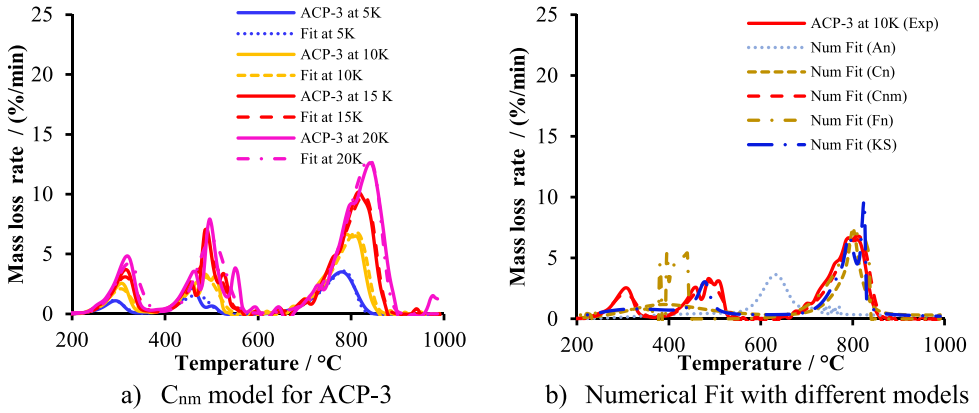

Fig. 11. DTG curve fitting of different models for ACP-3.

Table 6
Different models and their corresponding statistical significance for kinetics analysis.

Material	Types of method	Model/Code	R^2	The sum of dev. squares	Mean residual	F-test
ACP-1 (100% LDPE)	Model-free	FR	0.99966	1077.47	0.55	1.40
		K-A-S	0.95263	146670.69	3.25	191.08
		NOA	0.99976	767.60	0.48	1.00
		O-F-W	0.99741	8193.69	1.09	10.68
		VA	0.99965	1117.01	0.56	1.45
ACP-2 (30% LDPE co-polymer)	Model-based	[a]An	0.99984	200.54	0.27	4.22
		[b]Cn	0.99832	2053.68	0.62	43.38
		[c]Cnm	0.99989	130.24	0.21	2.76
		[d]Fn	0.99942	704.14	0.47	14.82
		[e]KS	0.99605	4825.29	1.18	102.61
ACP-3 (7% LDPE)	Model-based	[a]An	0.95469	10451.48	3.11	2791.65
		[b]Cn	0.99711	680.15	0.69	182.65
		[c]Cnm	0.99970	70.85	0.23	19.13
		[d]Fn	0.99290	1669.70	0.88	445.99
		[e]KS	0.99853	345.58	0.50	93.81

Here, a=Nucleation reaction of Avrami-Erofeev, b= Autocatalysis reaction, c= Modified autocatalysis reaction, d= Function of n^{th} order reaction, e= Kamal-sourur reaction.

3.3. Analysis of kinetics data

Kinetics analysis was conducted utilising the FR model for ACP-1 and the Cnm model for ACP-2 and ACP-3. The obtained kinetics parameters for the ACP-1, ACP-2, and ACP-3 samples using these models were provided in Table 7 and elaborated upon in the subsequent subsections.

The kinetics triplets of ACP-1 were determined using the FR model, yielding an average activation energy of 204.8 kJ/mol. This value falls within the reported literature range of 190–215 kJ/mol [59–61]. The pre-exponential factors were determined to have a value of 12.2 (log A [1/s]). Fig. 9(a) illustrates a comparison between the predicted curves generated by the FR model at various heating rates and the experimental DTG curves for ACP-1. The results indicate a good fit between the predicted actual test curves. Notably, the ACP-1 samples exhibited a single-stage reaction characterised with random chain scission [15,59,62]. The breakdown of the C-C bond of LDPE is the determining reaction and can be described as:

$$a \xrightarrow{R1} b + gas \tag{7}$$

Where a= initial reactant, b = product, and R1 = $LDPE_{solid} \xrightarrow{volatiles} LDPE_{volatile} + CO_2$.

The ACP-2 sample contains more than one component in the composite structure, showing multiple reaction steps (Fig. 10a). Four different reaction steps were found during curve fitting and pyrolysis analysis using the DTG peaks for mass loss rate (%/min). The best-fitting curve was found for the Cnm model. It is a feature of an autocatalytic reaction model. It is frequently used to parameterise the heterogeneous kinetics of complex polymers accurately and can resemble the kinetics of autocatalytic reactions. The autocatalytic model is also a foundation of the Kamal reaction model [63]. A multi-step reaction scheme is used in the present study (details in Appendix A1). The current model reaction scheme can be as follows:

$$a \xrightarrow{R1} b \xrightarrow{R2} c \xrightarrow{R3} d \xrightarrow{R4} e \tag{8}$$

Where,

$$R1 = (LDPE - VA)_{solid} + 2Al(OH)_3 \xrightarrow{dehydration} (LDPE - VA)_{melt} + Al_2O(OH)_4 + H_2O$$

$$R2 = (LDPE - VA)_{melt} + Al_2O(OH)_4 \xrightarrow{dehydration} (LDPE - VA)_{melt} + 2(AlOOH) + H_2O$$

$$R3 = (LDPE - VA)_{melt} + 2(AlOOH) \xrightarrow{release\ \ of\ \ volatiles} (LDPE - VA)_{Volatile} + \chi \quad Al_2O_3 + H_2O + CO_2$$

$$R4 = \chi \quad Al_2O_3 \xrightarrow{Phase\ \ transition} \gamma \quad Al_2O_3$$

In accordance with the above information, the first reaction, *R1*, with the value of $E_a = 124.22$ kJ/mol, log $A = 8.96$. It is assumed that this reaction step is the reason for the partial transformation of gibbsite to boehmite. The second reaction steps *R2* decomposition of gibbsite to boehmite, otherwise to χ-Al_2O_3 with activation energy, $E_a = 236.42$ kJ/mol, log $A = 14.45$ [64]. The third reaction step can be the possible outcome of LDPE-VA decomposition with activation energy, $E_a = 205.25$ kJ/mol and log $A = 12.70$. The fourth and final reaction valued with $E_a = 167.67$ kJ/mol and log $A = 10.53$ can be the phase transition of ATH from crystalline to amorphous alumina without any mass loss [65]. The effective activation energy E_a, log A, reaction order and other kinetics parameters can be found in Table 7. The reaction order *(n)* and autocatalytic pre-exponential constant *(p)* provide additional information on the chemical and physical reaction of the samples. The log value of *"p"*, describes the extent to which the decomposition reaction act as a self-catalyst for the reaction. Therefore, from Table 7 it can be seen that the obtained value of *"p"* is higher in *R3*, where the effect of thermal decomposition of LDPE-VA starts to decomposition. The free radicals of the polymer attack the other part of the polymer for degradation. The autocatalytic power showed higher values than the reaction rate, implying a slow degradation process of the composites.

ACP-3 showed similar numbers of reaction steps (Fig. 11a) to ACP-2, but one independent action was found with three continuous reaction steps (details in Appendix A2).

The current model reaction scheme can be as follow:

$$a \xrightarrow{R1} b \xrightarrow{R2} c \xrightarrow{R3} d \tag{9}$$

Table 7
Kinetics parameters of tested samples with different models.

Material	Model	E_a (kJ/mol)	log A *(A/1/s)*	n_i	c_i	p_i	m_i
ACP-1 (100% LDPE)	FR	R1 = 204.81	R1 = 12.2	-	-	-	-
ACP-2 (30% LDPE)	Cnm	R1 = 124.22	R1 = 8.957	R1 = 2.75	R1 = 0.39	R1 = 2.13	R1 = 8.30
		R2 = 236.42	R2 = 14.45	R2 = 1.63	R2 = 0.46	R2 = 2.44	R2 = 5.68
		R3 = 205.25	R3 = 12.69	R3 = 1.68	R3 = 0.05	R3 = 3.16	R3 = 5.57
		R4 = 167.67	R4 = 10.53	R4 = 2.97	R4 = 0.10	R4 = 2.81	R4 = 5.50
ACP-3 (7% LDPE)	Cnm	R1 = 105.00	R1 = 7.07	R1 = 2.93	R1 = 0.18	R1 = 0.06	R1 = 1.11
		R2 = 212.64	R2 = 12.72	R2 = 1.75	R2 = 0.22	R2 = 0.09	R2 = 4.16
		R3 = 89.66	R3 = 10.95	R3 = 2.20	R3 = 0.01	R3 = 2.33	R3 = 0.30
		R4 = 236.36	R4 = 9.11	R4 = 0.92	R4 = 0.59	R4 = 0.01	R4 = 10.00

E_a = Activation energy, A = pre-exponential factor, R_i =Reaction rate, n_i= Reaction order, c_i= Contribution, p = Log (Autocat. PreExp), Autocat. Power = m and i = 1,2,34.

$$e \xrightarrow{R4} f \tag{10}$$

Where,

$$R1 = (LDPE)_{solid} + 2Al(OH)_3 + CaCO_3 \xrightarrow{dehydration} (LDPE)_{melt} + Al_2O(OH)_4 + CaCO_3 + H_2O$$

$$R2 = (LDPE)_{melt} + Al_2O(OH)_4 + CaCO_3 \xrightarrow{dehydration} (LDPE)_{melt} + 2(AlOOH) + CaCO_3 + H_2O$$

$$R3 = (LDPE)_{melt} + 2(AlOOH) + CaCO_3 \xrightarrow{release\ \ of\ \ volatiles} (LDPE)_{Volatile} + \chi \quad Al_2O_3 + CaCO_3 + H_2O + CO_2$$

$$R4 = \chi Al_2O_3 + CaCO_3 \xrightarrow{release\ of\ volatiles} \gamma Al_2O_3 + CaO + CO_2.$$

The first reaction showed activation energy, $E_a = 105$ kJ/mol and log $A = 7.07$, which is nearly the similar value found in the literature [51] for the decomposition of ATH, where partial gibbsite transforms to boehmite due to dehydration. However, as this reaction step proceeds slowly, the mass loss is hardly visible in the TGA curve [51]. The second reaction can be due to the decomposition of gibbsite to boehmite to χ-Al_2O_3 with activation energy, $E_a = 212.64$ kJ/mol and log $A = 12.72$. The third reaction step can be the resultant reaction value of LDPE and ATH. In this step, the LDPE decomposed fully. On the other hand, a phase change reaction happens in ATH. As a result, the activation energy showed a lower value of $E_a = 89.66$ kJ/mol compared to the sole LDPE activation energy $E_a = 204.81$ kJ/mol. The final independent reaction step was observed due to the presence of $CaCO_3$. The value of activation energy E_a was 236.36 kJ/mol with a pre-exponential factor of log A= 9.11. The values match the literature, where the activation energy E_a of $CaCO_3$ can be found between 224 and 234 kJ/mol [66]. The higher value of autocatalytic pre-exponential constant, "p" indicates the effect of degradation of the LDPE polymer with autocatalytic reaction. In the case of reaction rate, n and autocatalytic power, m, it is evident that for R1 and R3, $n > m$. That means autocatalytic reaction plays a vital role in this step for the degradation of the samples.

3.4. Fire performance analysis

The burning behaviour of ACP core materials varies depending on their formulation (Table 8). Materials that are pure or nearly pure thermoplastics behave as non-charring solids, such as ACP-1 samples are characterised by very rapid ignition time (35 s), with no residue (Fig. 12**a**), and high heat release rate (1280 kW/m^2) in Fig. 13. However, ACP cores containing inorganic filler tend to have lower heat release (200–247 kW/m^2) but nearly the same ignition time **(**Fig. 13**)**. The presence of similar types of organic polymer (LDPE) can be the cause of identical ignition time. The percentage of polymer present in each sample strongly influenced the THR, EHC, and MLR values of the tested samples. As a result, ACP-1, with 100% organic polymer showed a maximum total heat release of 114 MJ/m^2, whereas ACP-2 and ACP-3, with 30% and 7% polymer exhibited a total heat release of 55 MJ/m^2 and 15 MJ/m^2, respectively. When comparing samples with 100% polymer to samples with organic fillers (7%), the effective heat of the combustion nearly doubled. Likewise, the same trends were found for the results of the mass loss rate of the samples. Samples ACP-2 and ACP-3 behaved similarly to charring materials as a char layer built up and insulated the underlying virgin material from external heat. The line cracks are shown in the ACP-2 char surface (Fig. 12b), whereas ACP-3 revealed the existence of cracks in the form of bubbles (Fig. 12c).

Samples ACP-2 and ACP-3 both showed two peaks during the burning (Fig. 13). The first peak originated from the surface ignition, and the later peak was responsible for the burning of interfacial polymer presented in the composite matrix. Both peaks were higher for ACP-2 compared to ACP-3. In the case of the burning duration, ACP-2 showed a higher burning duration (535 s) than ACP-3 (203 s). Note that in real cladding fire scenarios, the difference in the ignition time became less important under the heat flux above 100 kW/m^2, like in a post-flashover fire. However, the burning duration will be of higher relevance. Thus, a higher peak heat release rate and longer burning duration of ACP-2 core materials showed a more significant fire hazard compared to ACP-3. Thus, from the viewpoint of HRR, the fire hazard of ACPs core samples followed the polymer % fire hazard ranking. More importantly, the peak HRRPUA of ACP-2 and ACP-3 was also found to be higher than other common flammable materials, such as timber wood (150–200 kW/m^2) [67], polyisocyanurate foam (139 kW/m^2) [68], and PVC floor tile (181 kW/m^2) [68], although lower than ACP-1 (1280 kW/m^2). Therefore, even under the small lab-test scale, the fire hazard of these ACPs core materials may still be a primary concern due to its fast-developed market.

3.5. Validation of kinetics data

In order to verify the pyrolysis kinetics and further examine the flame behaviours of the investigated samples, samples (ACP-1, ACP-2, and ACP-3) were employed in Cone calorimeter modelling. In Fig. 14, the HRR values for simulated and experimental results were compared. Overall, the peak stages were accurately predicted by the numerical models. Table 9 summarised the flammability properties for both experimental and numerical results. The results showed that the ignition time of the samples were predicted with discrepancies ranging between 2 and 15 s. Minor underprediction of pHRR value was observed for numerical simulation compared to the experimental value of ACP-1 samples. However, for ACP-2, the first peak in the experiment was 247 kW/m^2, whereas the numerical peak value was 287 kW/m^2. Additionally, the 2nd peak value for the experiment was 172 kW/m^2 and the numerical 142 kW/m^2, which showed only the relative difference of 40 kW/m^2. The deviation in the results could be the reason for the complex function

Table 8
Flammability properties of different ACP samples.

Flammability properties	Sample code		
	ACP-1	ACP-2	ACP-3
TTI (s)	35	40	40
pHRR (kW/m^2)	1280	247 *	128 *
		172**	200**
Time to pHRR (s)	135	97 *	75 *
		420**	152**
EHC (MJ/kg)	42.00	23.21	22.53
THR (MJ/m^2)	114	55	15
Specific MLR (g/s.m^2)	21.26	5.64	4.32

Note: "–" = no ignition, * = 1st peak, * *= 2nd peak

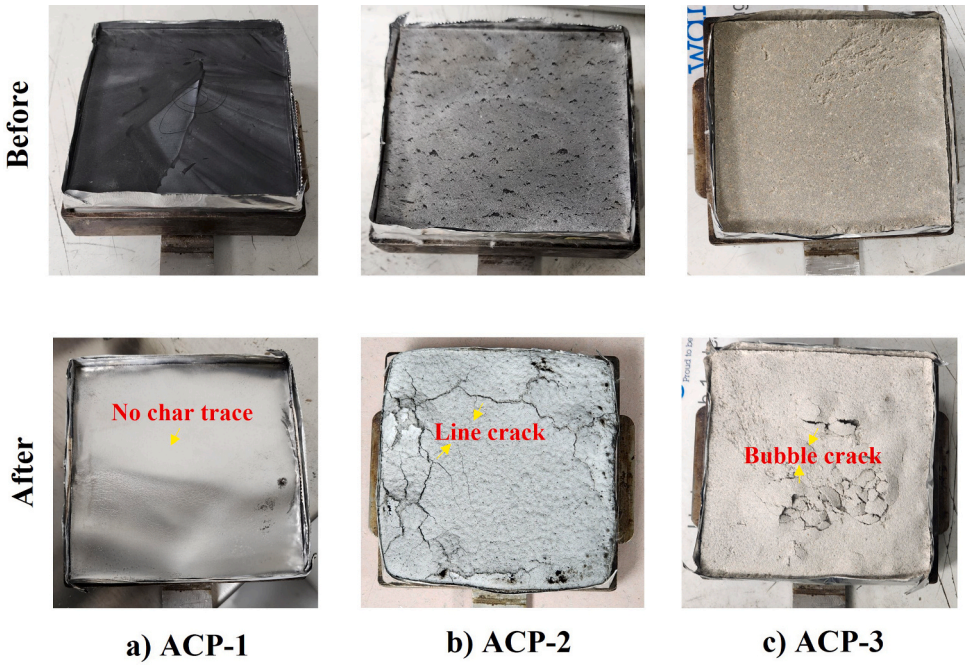

Fig. 12. Visual observation of the different materials of the cladding system before and after the test.

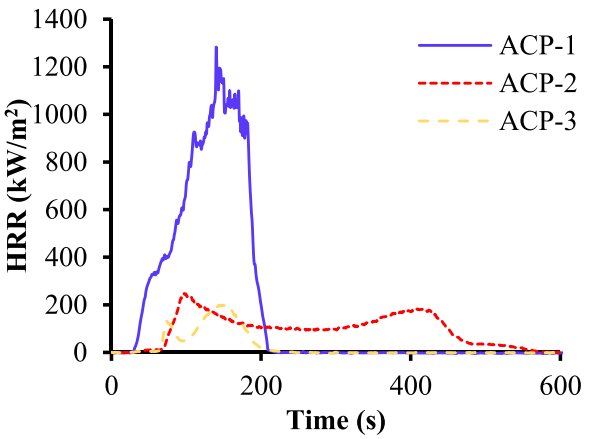

Fig. 13. Heat release rate of the different materials used in the cladding system.

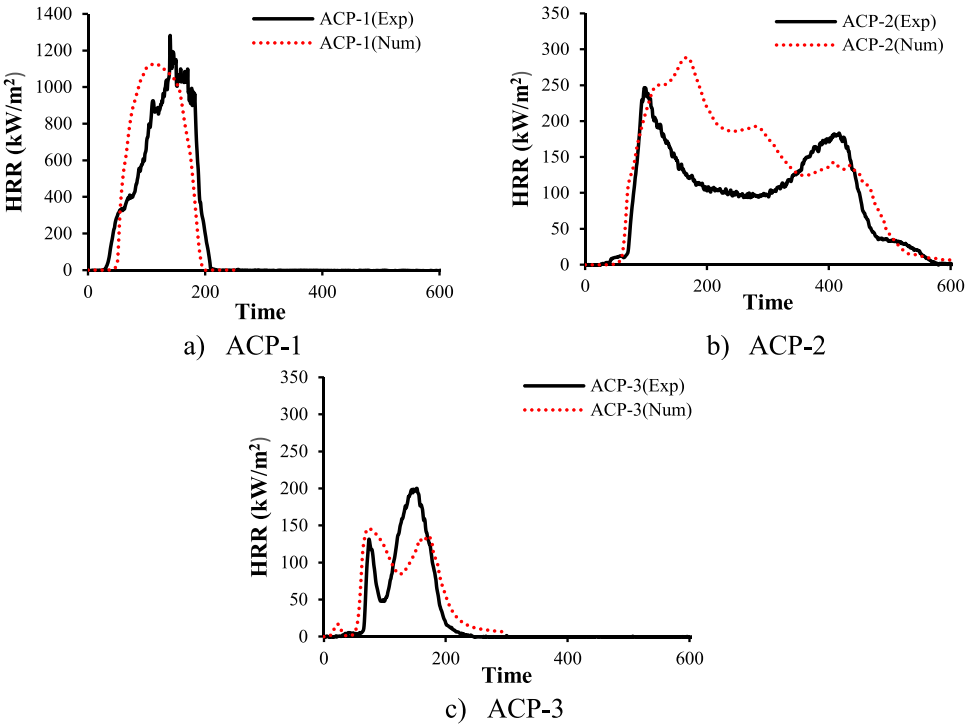

Fig. 14. Comparisons of numerical simulation against experimental HRR (a-c) of different cladding materials.

of the intumescent materials of the composites, which was complex to include in modelling and hence ignored. For ACP-3, the peaks and the time to the peak heat release rate were reasonably well predicted. On the other hand, comparing the visual flame to an experimental snapshot taken at the appropriate time intervals, a matched fire shape was seen (Fig. 15). Analysis of the flame height from the experimental Cone calorimeter was difficult because of the test design and settings. However, numerical models allow for more accurate analysis and comparison of flame height to the flammability of the test product. Finally, the numerical findings demonstrate that the model accurately represents ignition/extinction, fame spread, and combustion during pyrolysis. It could also mimic the size and flashing motion of the flames, as demonstrated in the experiment (Fig. 15).

4. Conclusion

This research study analysed the kinetics parameters and thermo-chemical reaction stages of cladding materials (ACP-1, ACP-2, and ACP-3). A systematic framework for extracting kinetics data from cladding materials for real-scale fire modelling was presented. Finally, the reaction to fire properties of cladding materials were examined and simulated to establish the optimised kinetics data for flame retardant cladding composites. In comparison to ACP-2 and 3, ACP-1 underwent more severe thermal degradation. The study uncovers the complexity of kinetics with ACP-1 displaying a single reaction step, while ACP-2 and ACP-3 exhibit multi-step

Table 9
Numerical and experimental data of different flammability properties.

Properties	ACP-1			ACP-2			ACP-3		
	Exp	Num	Δ	Exp	Num	Δ	Exp	Num	Δ
Ignition time (s)	35	50	15	40	42	02	40	49	09
Burning duration (s)	172	150	22	535	560	25	203	254	51
Extinguishment (s)	207	200	7	575	600	25	243	303	60
1st pHRR (kW/m^2)	1280	1128	152	247	287	40	128	145	17
2nd pHRR (kW/m^2)	-	-	-	172	142	30	200	135	65
1st time to pHRR(s)	135	115	20	97	170	73	75	76	01
2nd time to pHRR(s)	-	-		420	442	22	152	170	18
1st pMLR (kg/s·m^2)	0.033	0.026	0.007	0.012	0.007	0.005	0.008	0.004	0.004
2nd pMLR (kg/s·m^2)	-	-		0.005	0.003	0.002	0.006	0.003	0.003
1st time to pMLR(s)	165	110	55	105	166	61	79	72	077
2nd time to pMLR(s)	-	-		423	422	01	156	167	11

Δ = absolute relative difference

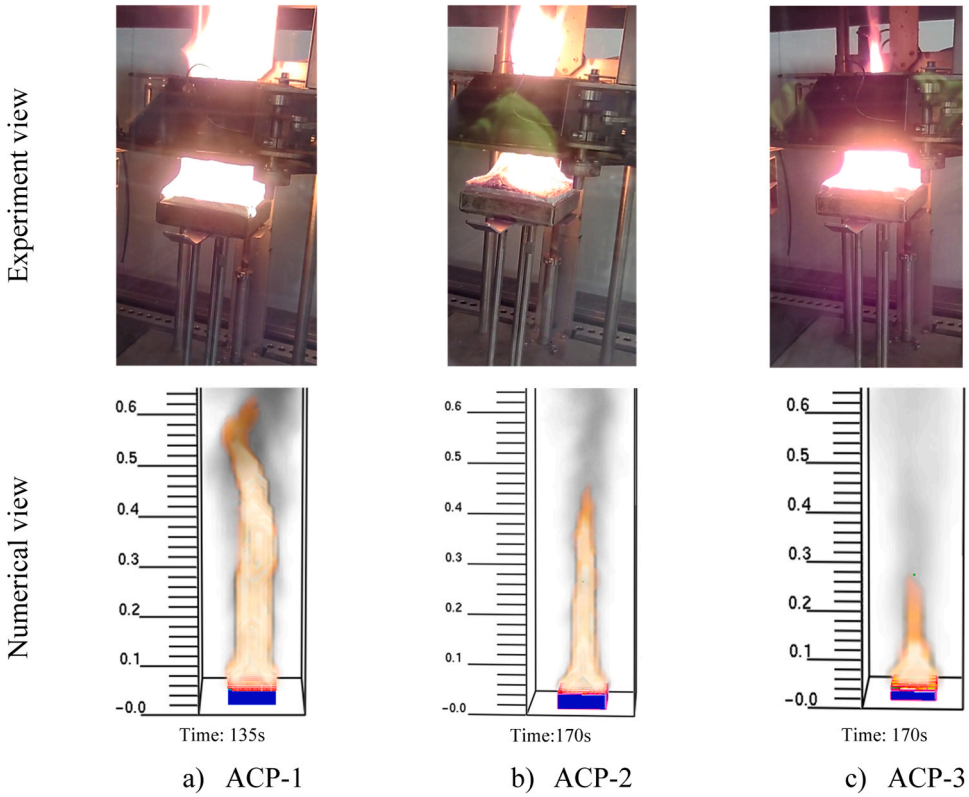

Fig. 15. Experimental and numerical visualisation of different ACP core materials during peak stage.

reactions, providing fresh insights into the behaviour of flame-retardant cladding composites. In the case of ACP-2, all the reaction steps were continuous, whereas three (03) continuous stages with one (01) independent step were observed in ACP-3. Additionally, the study introduces novel best-fit models for kinetics, enhancing our ability to predict fire retardant cladding composites responses accurately. The FR model was shown to be a best-fit kinetics model for ACP-1. Cnm model was determined to be the best match kinetics model for ACP-2 and − 3. The numerical results using kinetics data showed the capabilities of the numerical models to accurately represent ignition/extinction, flame spread, and combustion during pyrolysis of the core materials of ACPs from small-scale Cone calorimeter test data. The percentage of polymer in each sample showed substantial impact on key flammability parameters such as THR (Total Heat Release), EHC (Effective Heat of Combustion), and MLR (Mass Loss Rate) as determined through cone calorimetry. When the samples were compared containing 100% polymer to those incorporating organic fillers (7% of polymer), it was observed a nearly twofold increase in the EHC values. Both Samples ACP-2 and ACP-3 exhibited behaviour akin to charring materials, forming a protective char layer that insulated the underlying virgin material from external heat sources. However, ACP-2 displayed a higher pHRR and a longer burning duration compared to ACP-3, indicating a more significant fire hazard. Consequently, in terms of Heat Release Rate (HRR), the fire hazard ranking of ACP core samples corresponded directly to the percentage of polymer present. These findings collectively advance our knowledge and have significant implications for improving fire safety measures and modelling techniques in ACP cladding materials in building.

Declaration of Competing Interest

The authors declare that they have no known competing financial interests or personal relationships that could have appeared to influence the work reported in this paper.

Data Availability

The authors are unable or have chosen not to specify which data has been used.

Acknowledgements

This work is funded by the Australian Research Council (ARC) Industrial Transformation Training Centre (IC170100032) and Western Sydney University (P00024103). The authors would like to acknowledge the Advanced Materials Characterisation Facility

(AMCF) of Western Sydney University (WSU) and the ARC fire safety training centre, UNSW, Australia, for access to their instrumentation and help from staff. Special thanks to Dr Ric Wuhrer and Dr Laurel George from AMCF for their technical assistance and valuable discussion during the experiment.The authors sincerely appreciate all financial and technical support.

Appendix A

A1: Summary of model reaction scheme of ACP-2.
The balance equation:

$$Mass = m_i - \Delta m \times \left[ctb.(a\rightarrow b) \times \int\left[\frac{d(a\rightarrow b)}{dt}\right]dt + ctb.(b\rightarrow c) \times \int\left[\frac{d(b\rightarrow c)}{dt}\right]dt + ctb.(c\rightarrow d) \times \int\left[\frac{d(c\rightarrow d)}{dt}\right]dt + ctb.(d\rightarrow e) \times \int\left[\frac{d(d\rightarrow e)}{dt}\right]dt\right] \tag{A11}$$

Here, m_i= initial mass, Δm = total mass change, $ctb.$= contribution.
The rate equations in respect to each reaction step, considering C_{nm} model, can be presented as

$$\text{Reaction step R1}, \left(a \xrightarrow{R1} b\right): \quad \frac{d(a\rightarrow b)}{dt} = A_1 \times a^{n_1}\left(1 + k_{cat_1}.b^{m_1}\right) \times \exp\left[-\frac{E_{A_1}}{RT}\right] \tag{A12}$$

$$\text{Reaction step R2}, \quad b \xrightarrow{R2} c: \frac{d(b\rightarrow c)}{dt} = A_2 \times b^{n_2}\left(1 + k_{cat_2}.c^{m_2}\right) \times \exp\left[-\frac{E_{A_2}}{RT}\right] \tag{A13}$$

$$\text{Reaction step R3}, c \xrightarrow{R3} d: \frac{d(c\rightarrow d)}{dt} = A_3 \times c^{n_3}\left(1 + k_{cat_3}.d^{m_3}\right) \times \exp\left[-\frac{E_{A_3}}{RT}\right] \tag{A14}$$

$$\text{Reaction step R4}, d \xrightarrow{R4} e: \frac{d(d\rightarrow e)}{dt} = A_4 \times d^{n_4}\left(1 + k_{cat_4}.e^{m_4}\right) \times \exp\left[-\frac{E_{A_4}}{RT}\right] \tag{A15}$$

A2: Summary of model reaction scheme of ACP-3.
The balance equation:

$$Mass = m_i - \Delta m \times \left[ctb.(a\rightarrow b) \times \int\left[\frac{d(a\rightarrow b)}{dt}\right]dt + ctb.(b\rightarrow c) \times \int\left[\frac{d(b\rightarrow c)}{dt}\right]dt + ctb.(c\rightarrow d) \times \int\left[\frac{d(c\rightarrow d)}{dt}\right]dt + ctb.(e\rightarrow f) \times \int\left[\frac{d(e\rightarrow f)}{dt}\right]dt \quad \right] \tag{A21}$$

Here, m_i= initial mass, Δm = total mass change, $ctb.$= contribution.
The reaction rate equations for each reaction step, considering C_{nm} model, can be presented as follows:

$$\text{Reaction step R1}, \quad a \xrightarrow{R1} b: \quad \frac{d(a\rightarrow b)}{dt} = A_1 \times a^{n_1}\left(1 + k_{cat_1}.b^{m_1}\right) \times \exp\left[-\frac{E_{A_1}}{RT}\right] \tag{A22}$$

$$\text{Reaction step R2}, \quad b \xrightarrow{R2} c \quad \frac{d(b\rightarrow c)}{dt} = A_2 \times b^{n_2}\left(1 + k_{cat_2}.c^{m_2}\right) \times \exp\left[-\frac{E_{A_2}}{RT}\right] \tag{A23}$$

$$\text{Reaction step R3}, c \xrightarrow{R3} d: \frac{d(c\rightarrow d)}{dt} = A_3 \times c^{n_3}\left(1 + k_{cat_3}.d^{m_3}\right) \times \exp\left[-\frac{E_{A_3}}{RT}\right] \tag{A24}$$

$$\text{Reaction step R4}, e \xrightarrow{R4} f: \frac{d(e\rightarrow f)}{dt} = A_4 \times e^{n_4}\left(1 + k_{cat_4}.f^{m_4}\right) \times \exp\left[-\frac{E_{A_4}}{RT}\right] \tag{A25}$$

Appendix B

Nomenclature

k	Thermal conductivity of the material (W/m·K).
ρ	Density (kg/m^3).
C_p	Specific heat capacity (J/g·K).
α	Reaction conversion.
A	Pre-exponential factor (1/s).
E	Activation energy (kJ/mol).

R	Gas constant (J / K·mol).
β	Heating rate (K/min).
S^2	residual sum of squares.
R^2	Coefficient of determination.
$f(\alpha)$	Kinetic reaction model.
T	Absolute temperature (K).
t	Time (s).
ACP	Aluminium Composite Panel.
DSC	Differential Scanning Calorimetry.
DTG	Derivative of This Mass Loss Curve.
FDS	Fire Dynamics Simulator.
FR	Friedman.
FTIR	Fourier Transform Infrared.
KAS	Kissinger–Akahira–Sunose.
LDPE	Low-Density Polyethylene.
LDPE-VA	Low-Density Polyethylene Vinyl Acetate.
NOA	Numerical optimisation analysis.
OFW	Ozawa-Flynn-Wall.
STA	Simultaneous Thermal Analyser.
T_e	End temperature (°C).
TGA	Thermogravimetric Analysis.
T_o	Onset temperature (°C).
T_p	Peak temperature(°C).
VA	Vyazovkin.

Appendix C. Supporting information

Supplementary data associated with this article can be found in the online version at doi:10.1016/j.cscm.2023.e02535.

References

[1] M.D. Hossain, M.K. Hassan, A.C.Y. Yuen, Y. He, S. Saha, W. Hittini, Flame behaviour, fire hazard and fire testing approach for lightweight composite claddings–a review, J. Struct. Fire Eng. 12 (3) (2021) 257–292, https://doi.org/10.1108/JSFE-09-2020-0027.

[2] A.C.Y. Yuen, T.B.Y. Chen, I.M.D.C. Cordero, H. Liu, A. Li, W. Yang, S.C.P. Cheung, Q.N. Chan, S. Kook, G.H. Yeoh, Developing a solid decomposition kinetics extraction framework for detailed chemistry pyrolysis and combustion modelling of building polymer composites, J. Anal. Appl. Pyrolysis 163 (2022), 105500, https://doi.org/10.1016/j.jaap.2022.105500.

[3] N. White, Fire performance and test methods for ACP external wall cladding Australia(2020): CSIRO, Department of Environment L, Water and Planning; Contract No.: EP 196619.

[4] S.T. McKenna, N. Jones, G. Peck, K. Dickens, W. Pawelec, S. Oradei, S. Harris, A.A. Stec, T.R. Hull, Fire behaviour of modern façade materials–Understanding the Grenfell Tower fire, J. Hazard. Mater. 368 (2019) 115–123, https://doi.org/10.1016/j.jhazmat.2018.12.077.

[5] A.A. Khan, S. Lin, X. Huang, A. Usmani, Facade fire hazards of bench-scale aluminum composite panel with flame-retardant core, Fire Technol. (2021) 1–24, https://doi.org/10.1007/s10694-020-01089-4.

[6] BS 8414–1: Fire performance of external cladding systems. Test methods for non-loadbearing external cladding systems applied to the face of a building. UK., 2002.

[7] AS 5113:2016: Classification of external walls of buildings based on reaction-to-fire performance, 2016.

[8] S. Bakhtiyari, L. Taghi-Akbari, M.J. Ashtiani, Evaluation of thermal fire hazard of 10 polymeric building materials and proposing a classificationmethod based on cone calorimeter results, Fire Mater. 39 (1) (2015) 1–13, https://doi.org/10.1002/fam.2219.

[9] V.B. Apte, Flammability Testing of Materials Used in Construction, Transport and Mining, Woodhead Publishing, 2006.

[10] Y. Li, Z. Wang, X. Huang, An exploration of equivalent scenarios for building facade fire standard tests, J. Build. Eng. 52 (2022), 104399, https://doi.org/10.1016/j.jobe.2022.104399.

[11] Guillaume, Eric Fateh, Talal Schillinger, Renaud Chiva, Roman Ukleja, Sebastian, Study of fire behaviour of facade mock-ups equipped with aluminium composite material-based claddings, using intermediate-scale test method, Fire Mater. 42 (5) (2018) 561–577, https://doi.org/10.1002/fam.2635.

[12] A.C.Y. Yuen, T.B.Y. Chen, C. Wang, W. Wei, I. Kabir, J. Vargas, Q. Chan, S. Kook, G. Yeoh, Utilising genetic algorithm to optimise pyrolysis kinetics for fire modelling and characterisation of chitosan/graphene oxide polyurethane composites, Compos. Part B: Eng. 182 (2020), https://doi.org/10.1016/j.compositesb.2019.107619.

[13] K.T. Nguyen, S. Navaratnam, P. Mendis, K. Zhang, J. Barnett, H. Wang, Fire safety of composites in prefabricated buildings: from fibre reinforced polymer to textile reinforced concrete, Compos. Part B: Eng. 187 (2020), 107815, https://doi.org/10.1016/j.compositesb.2020.107815.

[14] D. Oswald, T. Moore, S. Lockrey, Combustible costs! financial implications of flammable cladding for homeowners, Int. J. Hous. Policy 22 (2) (2022) 225–250, https://doi.org/10.1080/19491247.2021.1893119.

[15] P. Das, P. Tiwari, Thermal degradation kinetics of plastics and model selection, Thermochim. Acta 654 (2017) 191–202, https://doi.org/10.1016/j.tca.2017.06.001.

[16] A. Aboulkas, A. El Bouadili, Thermal degradation behaviors of polyethylene and polypropylene. Part I: pyrolysis kinetics and mechanisms, Energy Convers. Manag. 51 (7) (2010) 1363–1369, https://doi.org/10.1016/j.enconman.2009.12.017.

[17] I. Dubdub, M. Al-Yaari, Pyrolysis of low density polyethylene: kinetic study using tga data and ann prediction, Polymers 12 (4) (2020) 891, https://doi.org/10.3390/polym12040891.

[18] P. Budrugeac, A. Cucos, R. Dascălu, I. Atkinson, P. Osiceanu, Application of model-free and multivariate nonlinear regression methods for evaluation of the kinetic scheme and kinetic parameters of thermal decomposition of low density polyethylene, Thermochim. Acta 708 (2022), 179138.

[19] T.B.Y. Chen, A. Yuen, G. Yeoh, W. Yang, Q. Chan, Fire risk assessment of combustible exterior cladding using a collective numerical database, Fire 2 (1) (2019) 1–14, https://doi.org/10.1016/j.tca.2021.179138.

[20] V. Dréan, B. Girardin, E. Guillaume, T. Fateh, Numerical simulation of the fire behaviour of facade equipped with aluminium composite material-based claddings-model validation at large scale, Fire Mater. 43 (8) (2019) 981–1002, https://doi.org/10.1002/fam.2759.

[21] V. Dréan, B. Girardin, E. Guillaume, T. Fateh, Numerical simulation of the fire behaviour of façade equipped with aluminium composite material-based claddings—model validation at intermediate scale, Fire Mater. 43 (7) (2019) 839–856, https://doi.org/10.1002/fam.2745.

[22] T. Rogaume, Thermal decomposition and pyrolysis of solid fuels: objectives, challenges and modelling, Fire Saf. J. 106 (2019) 177–188, https://doi.org/10.1016/j.firesaf.2019.04.016.

[23] Kinetics Neo. https://kinetics.netzsch.com/en (Accessed 4 July 2022).

[24] D. Oswald, T. Moore, S. Lockrey, Combustible costs! financial implications of flammable cladding for homeowners, Int. J. Hous. Policy (2021) 1–21, https://doi.org/10.1080/19491247.2021.1893119.

[25] Cladding Ban in NSW. Property Council of Australia.https://www.propertycouncil.com.au/Web/Content/News/NSW/2018/Cladding_Ban_in_NSW.aspx (Accessed 9 June 2020).

[26] Md. Delwar Hossain, Swapan Saha, Md. Kamrul Hassan, Anthony Chun Yin Yuen, Cheng Wang, W. Hittini, Influencing factors in small-scale fire testing of aluminium composite panels, 12th Asia-Oceania Symposium on Fire Science and Technology (AOSFST 2021), The University of Queensland, Brisbane, Australia, 2021.

[27] M. O'neill, Measurement of specific heat functions by differential scanning calorimetry, Anal. Chem. 38 (10) (1966) 1331–1336, https://doi.org/10.1021/ac60242a011.

[28] The Material Library of Cladding Materials. UQ eSpace. Data Collection. https://doi.org/10.14264/uql.2019.441 (Accessed 4 June 2021).

[29] J. Torero, Flaming ignition of solid fuels, SFPE handbook of fire protection engineering, Springer, 2016, pp. 633–661.

[30] L. Liu, T.B.Y. Chen, A.C.Y. Yuen, P.M. Doley, C. Wang, B. Lin, J. Liang, G.H. Yeoh, A systematic approach to formulate numerical kinetics for furnishing materials fire simulation with validation procedure using cone/FT-IR data, Heat. Mass Transf. (2021) 1–19, https://doi.org/10.1007/s00231-021-03144-4.

[31] M. Rashid, K. Chetehouna, A. Settar, J. Rousseau, C. Roudaut, L. Lemée, Z. Aboura, Kinetic analysis of the thermal degradation of an intumescent fire retardant coated green biocomposite, Thermochim. Acta 711 (2022), 179211, https://doi.org/10.1016/j.tca.2022.179211.

[32] J.D. Menczel, R.B. Prime, Thermal analysis of polymers: fundamentals and applications, John Wiley & Sons, 2009.

[33] K. Phuakpunk, B. Chalermsinsuwan, S. Assabumrungrat, Comparison of chemical reaction kinetic models for corn cob pyrolysis, Energy Rep. 6 (2020) 168–178, https://doi.org/10.1016/j.egyr.2020.08.041.

[34] A. Alonso, M. Lázaro, P. Lázaro, D. Lázaro, D. Alvear, Assessing the influence of the input variables employed by fire dynamics simulator (FDS) software to model numerically solid-phase pyrolysis of cardboard, J. Therm. Anal. Calorim. 140 (1) (2020) 263–273, https://doi.org/10.1007/s10973-019-08804-6 (0123456789).,(-volV)(0123456789).

[35] J. Ira, L. Hasalová, V. Šálek, M. Jahoda, V. Vystrčil, Thermal analysis and cone calorimeter study of engineered wood with an emphasis on fire modelling, Fire Technol. 56 (3) (2020) 1099–1132, https://doi.org/10.1007/s10694-019-00922-9.

[36] V. Mortezaeikia, O. Tavakoli, M.S. Khodaparasti, A review on kinetic study approach for pyrolysis of plastic wastes using thermogravimetric analysis, J. Anal. Appl. Pyrolysis 160 (2021), 105340, https://doi.org/10.1016/j.jaap.2021.105340.

[37] J. Cai, D. Xu, Z. Dong, X. Yu, Y. Yang, S.W. Banks, A.V. Bridgwater, Processing thermogravimetric analysis data for isoconversional kinetic analysis of lignocellulosic biomass pyrolysis: case study of corn stalk, Renew. Sustain. Energy Rev. 82 (2018) 2705–2715, https://doi.org/10.1016/j.rser.2017.09.113.

[38] M.D. Hossain, M.K. Hassan, S. Saha, A.C.Y. Yuen, C. Wang, L. George, R. Wuhrer, Thermal and pyrolysis kinetics analysis of glass wool and XPS insulation materials used in high-rise buildings, Fire 6 (6) (2023) 231, https://doi.org/10.3390/fire6060231.

[39] J. Opfermann, Kinetic analysis using multivariate non-linear regression. I. Basic concepts, J. Therm. Anal. Calorim. 60 (2) (2000) 641–658.

[40] A. Di Bucchianico, Coefficient of determination (R^2), Encycl. Stat. Qual. Reliab. 1 (2008).

[41] K. McGrattan, S. Hostikka, R. McDermott, J. Floyd, C. Weinschenk, K. Overholt, Fire Dynamics Simulator User's Guide, Sixth edition.,, 1019, NIST Special Publication, 2016.

[42] T. Nyazika, M. Jimenez, F. Samyn, S. Bourbigot, Pyrolysis modeling, sensitivity analysis, and optimization techniques for combustible materials: a review, J. fire Sci. 37 (4–6) (2019) 377–433, https://doi.org/10.1177/07349041198527.

[43] N.M. Petterson, Assessing the feasibility of reducing the grid resolution in FDS field modelling (PhD thesis), University of Cantenbury, NZ, 2002.

[44] J. Yang, R. Miranda, C. Roy, Using the DTG curve fitting method to determine the apparent kinetic parameters of thermal decomposition of polymers, Polym. Degrad. Stab. 73 (3) (2001) 455–461, https://doi.org/10.1016/S0141-3910(01)00129-X.

[45] S. Vyazovkin, A.K. Burnham, L. Favergeon, N. Koga, E. Moukhina, L.A. Pérez-Maqueda, N. Sbirrazzuoli, ICTAC Kinetics Committee recommendations for analysis of multi-step kinetics, Thermochim. Acta 689 (2020), 178597, https://doi.org/10.1016/j.tca.2020.178597.

[46] Z. Wang, R. Wei, X. Ning, T. Xie, J. Wang, Thermal degradation properties of LDPE insulation for new and aged fine wires, J. Therm. Anal. Calorim. 137 (2) (2019) 461–471, https://doi.org/10.1007/s10973-018-7957-5.

[47] L. George, R. Wuhrer, D.J. Fanna, C. Rhodes, Q. Huang, Characterisation Techniques for the Identification of Composite Cladding Materials and their Thermal Properties, International Conference on Mechanical and Manufacturing Engineering Research and Practice, iCMMERP2019, Sydney, Australia, 2019.

[48] D. Redaoui, F. Sahnoune, M. Heraiz, A. Raghdi, Mechanism and kinetic parameters of the thermal decomposition of gibbsite Al (OH) 3 by thermogravimetric analysis, Acta Phys. Pol. A 131 (3) (2017), https://doi.org/10.12693/APhysPolA.131.562.

[49] K. McGarry, J. Zilberman, T.R. Hull, W.D. Woolley, Decomposition and combustion of EVA and LDPE alone and when fire retarded with ATH, Polym. Int. 49 (10) (2000) 1193–1198, https://doi.org/10.1002/1097-0126(200010)49:10<1193::AID-PI537>3.0.CO;2-0.

[50] S.A. Isarov, P.W. Lee, J.H. Towslee, K.M. Hoffman, R.D. Davis, J.M. Maia, J.K. Pokorski, DNA as a flame retardant additive for low-density polyethylene, Polymer 97 (2016) 504–514, https://doi.org/10.1016/j.polymer.2016.05.060.

[51] S. Hamdani, C. Longuet, J.-M. Lopez-Cuesta, F. Ganachaud, Calcium and aluminium-based fillers as flame-retardant additives in silicone matrices. I. Blend preparation and thermal properties, Polym. Degrad. Stab. 95 (9) (2010) 1911–1919, https://doi.org/10.1016/j.polymdegradstab.2010.04.013.

[52] A. Ashraf, H. Sattar, S. Munir, A comparative applicability study of model-fitting and model-free kinetic analysis approaches to non-isothermal pyrolysis of coal and agricultural residues, Fuel 240 (2019) 326–333, https://doi.org/10.1016/j.fuel.2018.11.149.

[53] N.A. Testing, Kinetic Analysis - Selection of Suitable Kinetic Methods & Models by means of Kinetics Neo Software, 2022. https://www.youtube.com/watch?v=tKi70BAz3z8 (Accessed 9 June 2023).

[54] P. Šimon, P. Thomas, T. Dubaj, Z. Cibulková, A. Peller, M. Veverka, The mathematical incorrectness of the integral isoconversional methods in case of variable activation energy and the consequences, J. Therm. Anal. Calorim. 115 (2014) 853–859, https://doi.org/10.1007/s10973-013-3459-7.

[55] N. Manić, B. Janković, V. Dodevski, Model-free and model-based kinetic analysis of Poplar fluff (Populus alba) pyrolysis process under dynamic conditions, J. Therm. Anal. Calorim. 143 (5) (2021) 3419–3438, https://doi.org/10.1007/s10973-020-09675-y.

[56] S. Mandal, N.K. Mohalik, S.K. Ray, A.M. Khan, D. Mishra, J.K. Pandey, A comparative kinetic study between TGA & DSC techniques using model-free and model-based analyses to assess spontaneous combustion propensity of Indian coals, Process Saf. Environ. Prot. 159 (2022) 1113–1126, https://doi.org/10.1016/j.psep.2022.01.045.

[57] A. Karpov, O. Korobeinichev, A. Bolkisev, A. Shaklein, A. Shmakov, A. Paletsky, M. Gonchikzhapov, Numerical study of polyethylene burning in counterflow: effect of pyrolysis kinetics and composition of pyrolysis products, Fire Mater. 42 (7) (2018) 826–833, https://doi.org/10.1002/fam.2638.

[58] M.N. Siddiqui, E.V. Antonakou, H.H. Redhwi, D.S. Achilias, Kinetic analysis of thermal and catalytic degradation of polymers found in waste electric and electronic equipment, Thermochim. Acta 675 (2019) 69–76, https://doi.org/10.1016/j.tca.2019.03.001.

[59] C.-H. Wu, C.-Y. Chang, J.-L. Hor, S.-M. Shih, L.-W. Chen, F.-W. Chang, On the thermal treatment of plastic mixtures of MSW: pyrolysis kinetics, Waste Manag. 13 (3) (1993) 221–235, https://doi.org/10.1016/0956-053X(93)90046-Y.

[60] B. Saha, A. Ghoshal, Model-free kinetics analysis of ZSM-5 catalyzed pyrolysis of waste LDPE, Thermochim. Acta 453 (2) (2007) 120–127, https://doi.org/10.1016/j.tca.2006.11.012.
[61] A. Aboulkas, K. El Harfi, A. El Bouadili, Pyrolysis of olive residue/low density polyethylene mixture: part i thermogravimetric kinetics, J. Fuel Chem. Technol. 36 (6) (2008) 672–678, https://doi.org/10.1016/S1872-5813(09)60003-7.
[62] A. Witkowski, A.A. Stec, T.R. Hull, Thermal decomposition of polymeric materials, SFPE handbook of fire protection engineering, Springer,, 2016, pp. 167–254.
[63] M.R. Kamal, Thermoset characterization for moldability analysis, Polym. Eng. Sci. 14 (3) (1974) 231–239, https://doi.org/10.1002/pen.760140312.
[64] P. Tavares Teles Araujo, S. Pereira da Silva Ribeiro, A. Landesmann, Experimental evaluation of tri-hydrated aluminium in fire-retardant properties of glass fibre reinforced polymers, Fire and Materials.https://doi.org/10.1002/fam.3047.
[65] M. Hancock, Principal types of particulate fillers: particulate-filled polymer composites, 2013, Rapra Technology, UK, 2013, p. 542.
[66] L. Fedunik-Hofman, A. Bayon, S.W. Donne, Comparative kinetic analysis of $CaCO_3$/CaO reaction system for energy storage and carbon capture, Appl. Sci. 9 (21) (2019) 4601, https://doi.org/10.3390/app9214601.
[67] Q. Xu, L. Chen, K.A. Harries, F. Zhang, Q. Liu, J. Feng, Combustion and charring properties of five common constructional wood species from cone calorimeter tests, Constr. Build. Mater. 96 (2015) 416–427, https://doi.org/10.1016/j.conbuildmat.2015.08.062.
[68] K. Carpenter, M. Janssens, Using heat release rate to assess combustibility of building products in the cone calorimeter, Fire Technol. 41 (2) (2005) 79–92.